International Journal of Engineering

Applications of Impedance Plane and Magnetic Differential Permeability in Microstructural Characterization of AISI D2 Tool Steel

S. Kahrobaee *, M. Kashefi

Department of Materials Science and Metallurgical Engineering, Engineering Faculty, Ferdowsi University of Mashhad, Mashhad, Iran

A B S T R A C T

Two nondestructive electromagnetic techniques, hysteresis loop and eddy current methodologies, have been used to characterize the microstructural changes of D2 tool steel in the course of quench and tempering treatments. To measure the retained austenite fraction in the quenched microstructure, six specimens were austenitized in the range of 1000-1130 °C. Samples austenitized at 1080 °C were also tempered in the range of 200-650 °C for characterization by eddy current and magnetic hysteresis loop outputs.. Impedance point movement and maximum differential permeability were measured as a function of austenitizing/tempering temperature to characterize the microstructural features. The study showed that good correlations exist between microstructural variations detected by destructive methods (hardness, XRD and microscopic observation) and outputs of the nondestructive techniques.

doi: *10.5829/idosi.ije.2015.28.02b.09*

1. INTRODUCTION

AISI D2 is a high-carbon, high-chromium cold work tool steel characterized by its high wear resistance, hardness, compressive strength and stability in hardening [1, 2]. The properties make the steel suitable for applications such as heavy-duty cutting tools (dies and punches).

In as quenched microstructure, the presence of high amounts of the unwanted soft phase of retained austenite (γr) poses a major problem which could negatively affect the desired mechanical properties such as hardness and wear resistancen [1-3]. As a result, controlling the amount of γ_r is one of the major challenges in the heat treatment of tool steels.

Tempering, as the final stage of the heat treatment, modifies the working properties of the quenched steel, producing a desirable combination of strength, hardness and toughness [4, 5]. Tempering could be divided into the following stages [6]: 1. Up to approximately 200 °C, formation of transition carbides and lowering of carbon content in the martensite structure [7-9]. 2. In the range of 200-400°C, dissolving ε carbides and independently nucleating cementite M_3C [9, 10]. 3. Above 300-400°C, transformation of the retained austenite to lower bainite [11]. 4. At temperatures above 450 °C, precipitation of secondary carbides in the form of M_7C_3, MC and M_2C from the elements such as Cr, V, and Mo, respectively [9, 12, 13]. Precipitation of carbides is the main reason for secondary hardening effect. 5. At temperatures above 600 °C, carbides start to spheroidize. The conventional methods for evaluating the microstructural changes occur during the tempering of tool steels are hardness measurement to detect secondary hardening [14], X-ray diffraction techniques for assessment of retained austenite [15] and metallographic examinations to evaluate the degree of carbide spheroidization [16]. These destructive methods are not normally utilized in quality inspection of the heat treated parts due to the high cost of the tests.

In recent years, there is a growing demand for fast and reliable nondestructive methods to be applied for materials characterization [17-20]. Magnetic/ electromagnetic techniques such as eddy current (EC) and hysteresis loop measurements with a high

*Corresponding Author's Email: M-kashefi@um.ac.ir (M. Kashefi)

sensitivity to microstructural changes have the potential as an alternative to the traditional methods for nondestructive microstructural examination of quenched and tempered steel parts [21].

Amongstvarious forms of presenting test results for eddy current nondestructive method, impedance plane is the most theoretically well-established one. Impedance plane and movement of the location of impedance point are common ways for the investigation of cracks in materials [22, 23]. Generally, changes in coil impedance with and without sample being inserted in the coil will be calculated to form impedance plane. The variables affecting the position of impedance point in the plane are resistance and reactance which change as a result of microstructural variations of the specimen being tested[21].

Bray et al. [22] and Shull [23] have theoretically investigated the effect of parameters such as lift off and resistance on impedance plane. Kashefi et al. have demonstrated the effect of decarburizing layer [24] and case depth [25] on impedance plane and illustrated the movement of impedance point in different conditions of heat treatment process. Tempered martensite embrittlement (TME) in high strength steel has also been detected using impedance point movement [26]. The effects of lift off and grain size of microstructure on the impedance plane have also been examined by Zergoug et al. [27]. They showed that the eddy current testing is sensitive to changes in microstructure for Al-Zn alloy and three types of steels. Foyet has studied the corrosion behavior of Al-2024 aluminum alloy coated with a chromate-free primer using impedance measurement[28]. Sheikh Amiri et al. [29] have studied the effect of surface carbon content and the variables affecting impedance plane, such as temperature, fill factor and edge effect on carburized steel.

Microstructural changes during tempering heat treatment of cold work tool steels are very complex due to the simultaneously occurring phenomena such as retained austenite decomposition and carbide precipitation. Thus, it is important to investigate the combined effects of the microstructural changes on electromagnetic outputs. In the present study, the effects of microstructural changes under different conditions of austenitizing and tempering temperatures of the AISI D2 steel on electrical resistivity (ρ) and differential permeability have been separately evaluated and their combined effects on the EC outputs have been taken into account.

2. EXPERIMENTAL PROCEDURE

The specimens $100 \times 21 \times 4$ mm in size were prepared from AISI D2 tool steel. Table 1 gives the chemical composition of the steel. The practical austenitizing temperatures for cold work tool steels are 1000 to 1130°C. Austenitization at six temperatures was done in a vacuum furnace to avoid oxidation and decarburization. Quenching was done in oil and tempering was performed at 5 different temperatures for 2 hours, as indicated in Table 2.

The samples were polished and etched with Vilella's reagent (2 g picric acid and 5 ml HCl in 100 ml ethyl alcohol) for metallographic investigations. The cross sections of the specimens were evaluated using a scanning electron microscope (SEM VP 1450).

Hardness was measured in Rockwell C scale at 5 locations for each specimen.

A four-probe method was used for electrical resistivity measurements on the samples with the dimension of $90 \times 4 \times 1$ mm.

The block-scheme of the home-made testing devices of the eddy current and magnetic differential permeability (μ_{Diff}) measurement systems are shown in Figure 1. The number of turns in the driving and pickup coils were 500 and 600, respectively. The pickup coil was placed in the center of the driving coil and the EC outputs (impedance points) were evaluated for different microstructures. For measurement of μ_{Diff}, the probe was made using a driving copper coil of 1000 turns and a pickup coil of 500 turns wound on a U-shaped ferrite core and the sample, respectively. The driving coil gets an amplified triangular waveform signal with stepwise increasing amplitudes and fixed slope magnitude. This, produces a triangular time-variation of the effective field, V1(t), in the magnetizing circuit which can be converted to the magnetic field strength.

TABLE 1. Nominal composition of the investigated AISI D2 steel

Elements	C	Si	Mn	P	S
Amount (wt%)	1.51	0.32	0.27	0.019	0.016
Elements	Cr	Mo	Ni	V	Fe
Amount (wt%)	11.60	0.63	0.20	0.91	Balance

TABLE 2. Applied heat treatment cycles

Heat Treatment	Austenitization	Tempering					
Temperature (°C)	1000 1025 1055 1080 1105 1130	200	300	400	500	580	650
Time (min)	30	120					

The induction signal for the hysteresis measurements was recorded by induced signals in the pick-up coil, V2 (t).

In order to plot B-H curve, the measured induced voltage was used to calculate the magnetic induction (B) according to the induction law[30]:

$$V_2(t) = -NA\frac{dB}{dt} \tag{1}$$

where A and N are the sample cross-section and number of turns round the pickup coil, respectively.

Equation 2 was also used to calculate the differential magnetic permeability (μ_{Diff}). The results were used to plot the μ_{Diff} curve as a function of magnetic field strength.

$$\mu_{Diff} = \frac{1}{\mu_0}\frac{dB}{dH} \tag{2}$$

where B is magnetic flux density, H magnetic field strength and μ_0 $4\pi \times 10^{-7}$ Henry/m.

3. RESULTS AND DISCUSSION

3. 1. Destructive Characterization   Figure 2 shows the scanning electron microscopic image of the sample quenched from austenitizing temperature of 1130°C. The microstructure consists of martensite (M), primary carbides (C) and retained austenite (γr).

Figure 3 shows the SEM images of the microstructures of the sample austenitized at 1080°C and tempered at 200, 580 and 650°C.
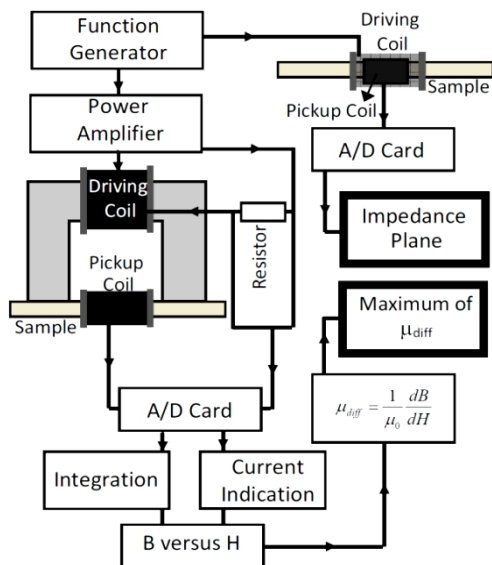

Figure 2. SEM image of the steel, austenitized at 1130 °C and quenched in oil

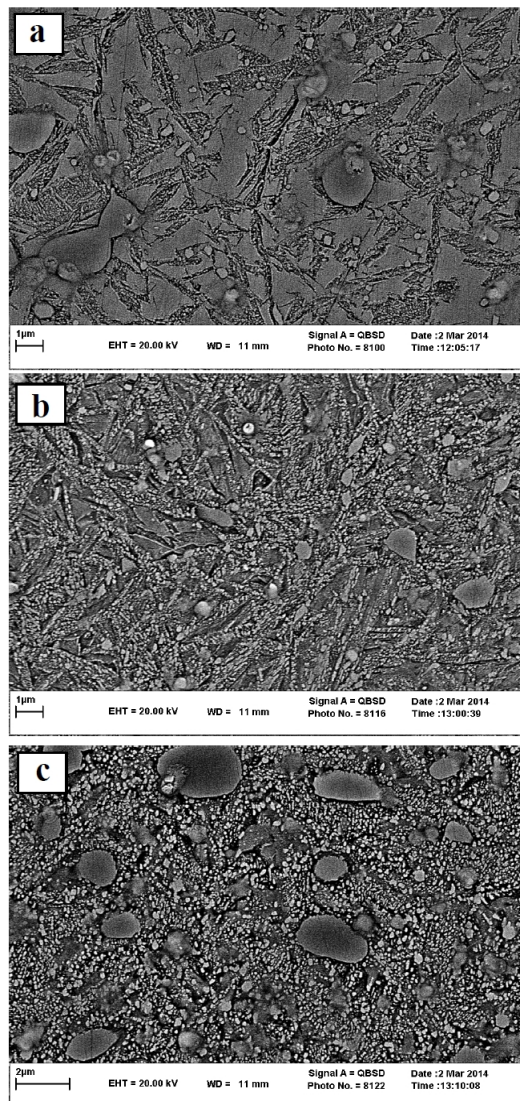**Figure 1.** Block-scheme of the EC and μ_{Diff} measurement system

Figure 3. SEM micrograph for samples austenitized at 1080 °C, quenched and tempered at a) 200 °C, b) 580 °C, and c) 650 °C

In the microstructure of the sample tempered at 200°C (Figure 3(a)), transition carbides (mainly ε carbide [9]) are formed from them artensite plates. In the sample tempered at 580 °C (Figure 3(b)), carbides are precipitated in all areas of the matrix, indicating the completion of the retained austenite decomposition. In this situation, the microstructure contains carbides distributed in the ferrite matrix. Figure 3(c) shows that as the tempering temperature rises to 650°C, the carbide precipitates are spheroidized.

XRD graph of the sample quenched from austenitizing temperature of 1080 °C is presented in Figure 4. Five peaks corresponding to 2θ angles of 43.47°, 50.67°, 74.67°, 90.67° and 95.94° are observed which are attributed to the (111), (200), (220), (311) and (222) planes of the austenite, respectively. The diffraction line coinciding with the (110), (200), (211) and (220) planes at 2θ = 44.67°, 65.02°, 82.33° and 98.94° were considered as martensite phase. The volume fractions of the retained austenite are calculated by comparing the integrated X-ray diffraction intensity of martensite and austenite phases. The volume fraction of total carbide content was first measured by image analysis techniques. The intense peaks of the martensite and austenite were then used to estimate the retained austenite content. Details of the procedure could be found in ASTM E975-03[31].

Results of the quantitative determination of the retained austenite for the quenched samples, presented in Figure 5(a), indicate a change in the volume fraction of γ_r from 15.7 to 42.0% with increasing austenitizing temperature. The increase in the amount of retained austenite is attributed to the increase in dissolved carbides at higher austenitizing temperatures. The presence of higher carbon and alloying elements in the austenite solid solution results in the further reduction of both Ms (martensite-start temperature) and Mf, and, in turn, a higher amount of retained austenite.
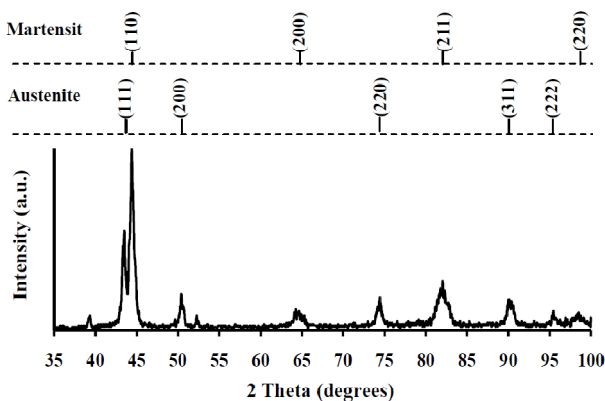

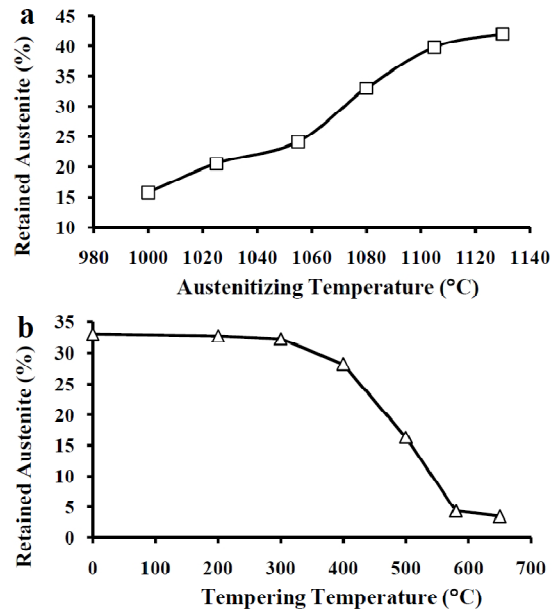**Figure 4.** X-ray diffraction pattern of austenitized sample at 1080 °C

Figure 5. Retained austenite fraction for samples a) austenitized at different temperatures, b) austenitized at 1080 °C and tempered at different temperatures

The amount of retained austenite in the samples austenitized at 1080 °C and tempered at different temperatures are also presented in Figure 5(b). It can be clearly seen that during tempering the amount of the retained austeniteremains constant up to 300°C, decreases in a low level at 400°C, reached to the approximately 50% of its primary value at 500°C and finally, disappears at 580 and 650°C. The figure shows that the decomposition of retained austenite has started above 300 °C. Variation in hardness for the samples austenitized and tempered at different temperatures is shown in Figure 6. As Figure 6(a) shows, the hardness of D2 steel increases with increasing the austenitizing temperature from 1000 to 1025°C, which is due to higher concentration of alloying elements in the matrix of the austenitized samples. In the next regime, from 1025 to 1130°C, the decrease in the hardness is related to the dominating effect of the retained austenite enhancement, or in other words, the decrease in the volume fraction of martensite. For samples austenitized at 1080°C and tempered at different temperatures, the hardness variations are as follows: a moderate reduction up to 400°C, an increase with a peak at 500°C followed by a drastic decrease at higher tempering temperatures (Figure 6 (b)). The initial moderate decrease in the hardness up to 400°C is attributed to the lowering of carbon content in the martensite structure as well as the reduction in dislocation density (due to the recovery mechanism) and microstresses [32].
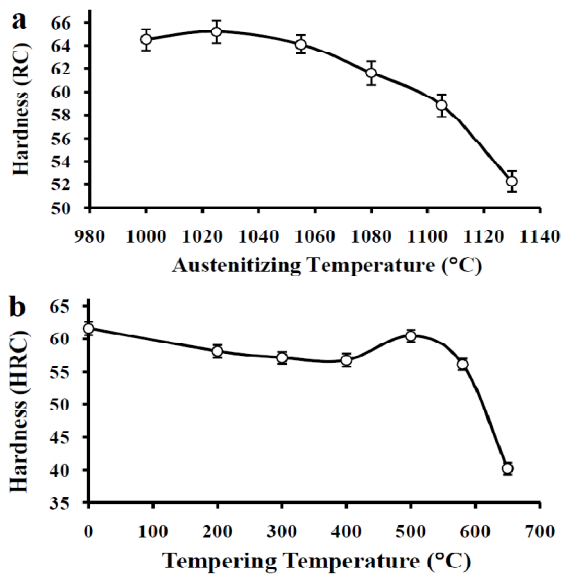
a

b

Figure 6. Variation of hardness for samples a) austenitized at different temperatures, b) austenitized at 1080°C and tempered at different temperatures

a

b

Figure 7. Variation of electrical resistivity for samples a) austenitized at different temperatures, b) austenitized at 1080°C and tempered at different temperatures

The peak in the hardness at 500°C is attributed to the precipitation of fine alloying carbides from the matrix. The subsequent decrease in the hardness with tempering at 580 °C is attributed to the formation of ferrite due to the complete decomposition of retained austenite. As the tempering temperature rises to 650°C, alloy carbides precipitate from the matrix, grow and start to spheroidize, and residual stresses are almost completely relieved, and hence the hardness is minimum.

Figure 7 shows the variation of electrical resistivity for samples austenitized and tempered at different temperatures. In the as-quenched samples (Figure 7(a)), the increase in electrical resistivity can be related to the increase in dissolving of alloying elements in the matrix as well as the presence of higher amounts of retained austenite at higher austenitizing temperatures.

Correlating electrical conductivity with tempering temperature (Figure 7(b)), the tendency is different: The resistivity curve shows three stages, i.e. a decrease up to 200°C and then leveling off up to 400°C, followed by a relative decrease at higher tempering temperature (beyond 400°C). Reduction during the initial stage is attributed to the removal of carbon from martensite and decrease in point defects and dislocations densities. Further decrease in the resistivity at higher temperatures (up to 580°C) can be attributed to precipitation of the alloying carbides due to the removal of chromium, vanadium and molybdenum from solid solution as well as decomposition of retained austenite having higher electrical resistivity than martensite. At final stage of tempering, spheroidization of carbides causes a reduction in the electrical resistivity.
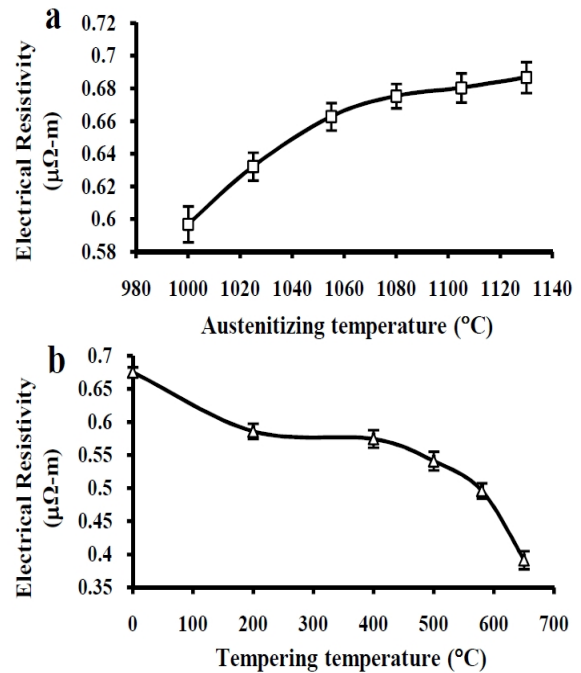
3. 2. Nondestructive Characterization

3. 2. 1. Differential Permeability
Variations of magnetic differential permeability (μ_{diff}) as a function of applied magnetic field for the samples austenitized and tempered at different temperatures are presented in Figure 8.

As can be seen in Figure 8(a), maximum μ_{diff} decrease with increase in austenitizing temperature; the highest and the lowest values of the maximum μ_{diff} were observed for the samples austenitized at 1000 and 1130°C, respectively.

The observed magnetic response is due to the reduction in ferromagnetic martensite volume fraction (from 77.0 to 53.2%) and an increase in concentration of carbon and alloying elements in the crystal structure of the matrix. Figure 8(b) shows μ_{diff} changes versus applied magnetic field for the samples tempered at 200, 300, 400, 500, 580 and 650°C.

As can be seen, the maximum μ_{diff} increased in a very low level with tempering at 200 and 300°C followed by an increase at 400 °C and then leveling off up to 500 °C. Finally, a continuous sharp increase can be seen at higher tempering temperatures. The initial increase in the maximum μ_{diff} up to 200-300°C is attributed to the reduction of carbon content in martensite due to the precipitation of ε carbides[9].
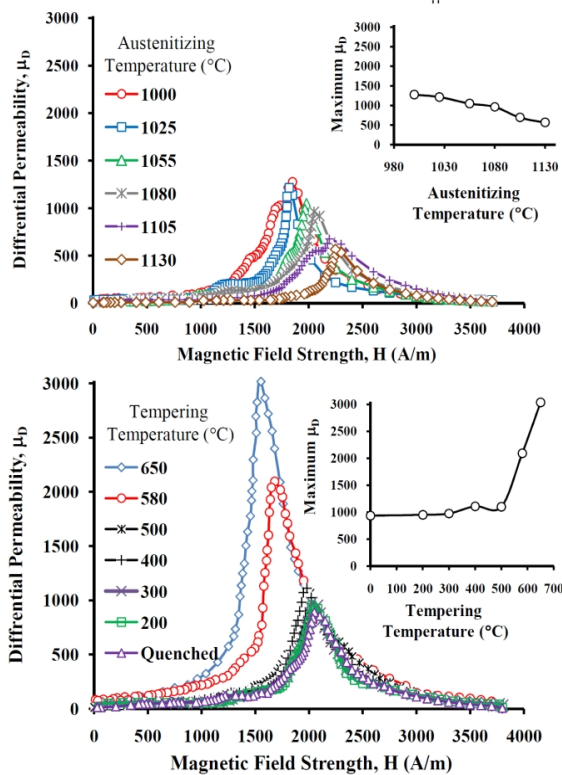
Figure 8. Differential permeability as a function of magnetic field strength for samples a) austenitized at different temperatures and b) austenitized at 1080 °C and tempered at different temperatures

An increase in the maximum μ_{diff} at 400°C is due to two factors: 1. A small amount of retained austenite is decomposed to bainite which have high fraction of soft magnetic ferrite, and 2. At 400°C, ε-carbides are replaced with cementite and thus, the crystal structure of martensite loses its tetragonality, and dislocation density reduces.

As observed, maximum μ_{diff} for the samples tempered at 400 and 500°C remained almost constant. This can be attributed to manifestation of two opposing mechanisms which take place simultaneously during tempering. The expected increase in maximum μ_{diff} due to the decomposition of retained austenite is compensated by the precipitation of secondary carbides. Formation of secondary carbides for samples tempered at 500°C, which was observed by secondary hardening effect (Figure 6(b)), provides obstacles to the movement of domain walls during magnetization. On the other hand, the reduction of paramagnetic retained austenite from 28.2 to 16.3% or, in other words, formation of bainite containing magnetically soft ferrite increases the maximum μ_{diff}, significantly.

By increasing the tempering temperature up to 580°C, as the decomposition of retained austenite is completed, a large increase in μ_{diff} can be seen (from 1100 to 2090). In this stage, the dominant effect on the drastic increase is attributed to the more favorable response of ferrite (matrix containing of carbides) to the applied magnetic field in comparison to the hard magnetically martensite and nonmagnetic retained austenite phases.

As presented in Figure 8(b), the highest maximum μ_{diff} reading was obtained for the sample tempered at 650°C. Since the decomposition of retained austenite completed at 580°C, spheroidization of carbides (as shown in Figure 3(c)) has a dominant effect on the maximum μ_{diff}. For the sample tempered at 580°C, the nature of pinning sites for domain walls is mainly determined by carbide lamellae in ferrite grains. The large interfacial area of carbide lamellae, which in turn, increases volume fraction of pinning sites, and subsequently increases the energy loss and restricts the movement of domain walls during the magnetization process. In carbide spheroidization process, average distance between pinning sites increases allowing domain walls to move more freely. These morphological changes as well as complete relief in residual stresses result in a drastic increase in the μ_{diff} from 2090 to 3040.

3. 2. 2. Impedance Plane   The details of the impedance plane calculations can be found elsewhere in literature [24, 33]. Impedance plane is formed by drawing normalized R (total resistance) as a function of normalized X (total reactance) which is shown in Figure 9. The normalized ones are calculated using Equations (3) and (4).

Normalized R=(R-R0)/X0   (3)

Normalized X=X/X0   (4)

where, R0 and X0 are the free space probe resistance and reactance, respectively.

Variables which can affect the position of impedance point in the plane are resistance and reactance. The results of calculations for characterization of tempered microstructures are presented in Figure 9.

• In the presence of the ferromagnetic sample, the probe inductance (reactive impedance) increases contrary to the EC effect, which decreases inductance. Simply, the magnetic flux density is in phase with the applied field for an increase in the magnetic permeability (μ_r) (neglecting hysteresis losses caused by the changing field), whereas the eddy current generated by the secondary magnetic field opposes the applied field. These two effects influence the impedance of the EC probe, independently. Therefore, for a ferromagnetic conductive sample, the total change in the EC probe inductance is the total resultant of the small decrease due to the reflected field from the induced eddy currents

and major increase due to the effect of large μ_r of the ferromagnetic sample.

- As shown in Figure 9(a), normalized R (which is equal to the resistive losses) decreases with austenitizing temperature. It is attributed to the increase in ρ, which in turn, reduces eddy current flow in the sample[23].

- Increasing the austenitizing temperature leads to an increase in the fraction of retained austenite which acts as strong pinning sites to domain wall motion. Thereby, a reduction in magnetic permeability is expected.

- As shown in Figure 9(b), normalized R increases with temping temperature which is due to the decrease in electrical resistivity (according to Figure 7(b)). Increase in μ_{diff} at 200-300°C tempering and subsequent increase in μ_{diff} at 400°C leads to an increase in the inductance. Increase in inductance at higher tempering temperatures is also attributed to the increase in the μ_{diff}.

According to Equations (5) and (6), inductance and reactance decrease with austenitizing temperature due to the decrease in μ_{diff} and increase with tempering temperatures as a result of increase in the μ_{diff}, (as observed in Figure 8).

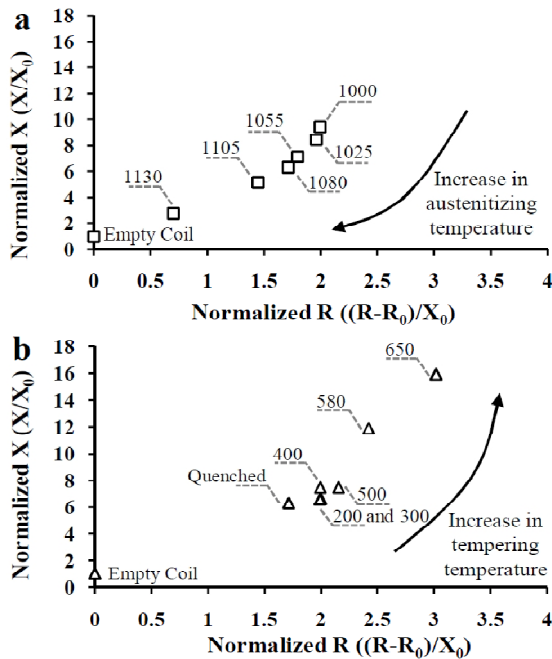$$L = \mu N^2 A / l \qquad (5)$$

$$X_L = 2\pi f L \qquad (6)$$

where L is coil inductance, μ the magnetic permeability, N the number of turns round the coil, A the cross sectional area, l the coil length, X_L reactance and f the frequency of applied current.

4. CONCLUSION

In the present paper, the microstructural changes due to application of different heat treatment cycles on AISI D2 tool steel have been evaluated by nondestructive eddy current and hysteresis loop measurements. The main conclusions from this work are as follows:

1. The points on impedance plane move downwards and maximum magnetic differential permeability decreases as the retained austenite fraction increases in quenched samples.

2. The relative changes of the differential permeability due to the tempering treatment were:

- A small increase (3 %) with tempering at 200 and 300°C due to the precipitation of   carbides and cementite, respectively.

- A moderate increase at 400°C (18%) related to the retained austenite decomposition. The constant value was obtained at 500°C which is attributed to the manifestation of two opposing agents, precipitation of alloying carbides and retained austenite decomposition.

- Finally, a sharp increase at 580°C (124%) and 650°C (225%) as a result of the complete decomposition of the retained austenite and the spheroidization of carbides, respectively.

3. A good agreement between destructive (hardness, XRD, microscopic observation) and nondestructive results showed the applicability of the electromagnetic/magnetic methods in microstructural characterization of the heat treated tool steel.

Figure 9. Impedance plane and effect of a) austenitizing temperature, and b) tempering temperature, on location of impedance point

5. REFERENCES

1. Roberts, G.A. and Kennedy, R., "Tool steels, ASM International, (1998).

2. Thelning, K.-E. and Black, C.M., "Steel and its heat treatment, Butterworths London, Vol. 1, (1984).

3. Totten, G.E. and Howes, M.A., "Steel heat treatment handbook, CRC Press, (1997).

4. Unterweiser, P.M., "Heat treater's guide: Standard practices and procedures for steel, Asm Intl, (1982).

5. Avner, S.H., "Introduction to physical metallurgy", (1964).

6. Carlson, E., "Cold treating and cryogenic treatment of steel in asm handbook, vol. 4 heat treating", *ASM International, 10th Ed., Metals Park, OH*, (1990), 203-206.

7. Hirotsu, Y. and Nagakura, S., "Crystal structure and morphology of the carbide precipitated from martensitic high carbon steel during the first stage of tempering", *ActaMetallurgica*, Vol. 20, No. 4, (1972), 645-655.

8. Williamson, D., Nakazawa, K. and Krauss, G., "A study of the early stages of tempering in an fe-1.2 pct alloy", *Metallurgical Transactions A*, Vol. 10, No. 9, (1979), 1351-1363.

9. Gavriljuk, V.G., Sirosh, V.A., Petrov, Y.N., Tyshchenko, A.I., Theisen, W. and Kortmann, A., "Carbide precipitation during tempering of a tool steel subjected to deep cryogenic treatment", *Metallurgical and Materials Transactions A*, Vol. 45, No. 5, (2014), 2453-2465.

10. J., P. and B., P., "Effect of tempering temperature on 30hgsa steel toughness", *Metallurgy and Casting*, Vol. 10, No., (1984), 409-421.

11. Kokosza, A. and Pacyna, J., "Evaluation of retained austenite stability in heat treated cold work tool steel", *Journal of Materials Processing Technology*, Vol. 162, No., (2005), 327-331.

12. Bała, P., Pacyna, J. and Krawczyk, J., "The kinetics of phase transformations during tempering of cr-mo-v medium carbon steel", *Journal of Achievements in Materials and Manufacturing Engineering*, Vol. 20, No. 1-2, (2007), 79-82.

13. Bała, P., Pacyna, J. and Krawczyk, J., "The influence of the kinetics of phase transformations during tempering on the structure development in a high carbon steel", *Archives of Metallurgy and Materials*, Vol. 52, No. 1, (2007), 113-120.

14. Handbook, M., "Heat treating", *vol*, Vol. 4, No., (1991), 744.

15. Tavares, S.S.M., Mello, S.R., Gomes, A.M., Neto, J.M., da Silva, M.R. and Pardal, J.M., "X-ray diffraction and magnetic characterization of the retained austenite in a chromium alloyed high carbon steel", *Journal of Materials Science*, Vol. 41, No. 15, (2006), 4732-4736.

16. Samuels, L.E., "Optical microscopy of carbon steels, American Society for Metals, (1980).

17. Farrahi, G.H. and Lebrun, J.L., "Surface hardness measurement and micro-structural characterization of steel by x-ray diffraction profile analysis", *International Journal of Engineering*, Vol. 8, No. 3, (1995), 159-167.

18. Farrahi, G.H., "The dc electrical potential method for the measurement of fretting cracks", *International Journal of Engineering*, Vol. 9, No. 1, (1996), 19-27.

19. Rakideh, M., Dardel, M. and Pashaei, M., "Crack detection of timoshenko beams using vibration behavior and neural network", *International Journal of Engineering-Transactions C: Aspects*, Vol. 26, No. 12, (2013), 1433.

20. Wang, Y. and Wu, Q., "Experimental detection of composite delamination damage based on ultrasonic infrared thermography", *International Journal of Engineering (1025-2495)*, Vol. 27, No. 11, (2014).

21. Hagemaier, D.J., "Fundamentals of eddy current testing, American Society for Nondestructive Testing, (1990).

22. Bray, D.E. and Stanley, R.K., "Nondestructive evaluation: A tool in design, manufacturing and service, CRC press, (1996).

23. Shull, P.J., "Nondestructive evaluation: Theory, techniques, and applications, CRC press, (2002).

24. Kashefi, M. and Kahrobaee, S., "Dual-frequency approach to assess surface hardened layer using nde technology", *Journal of materials engineering and performance*, Vol. 22, No. 4, (2013), 1108-1112.

25. Kashefi, M., Rafsanjani, A., Kahrobaee, S. and Alaee, M., "Magnetic nondestructive technology for detection of tempered martensite embrittlement", *Journal of Magnetism and Magnetic Materials*, Vol. 324, No. 23, (2012), 4090-4093.

26. Zergoug, M., Lebaili, S., Boudjellal, H. and Benchaala, A., "Relation between mechanical microhardness and impedance variations in eddy current testing", *NDT & E International*, Vol. 37, No. 1, (2004), 65-72.

27. Foyet, A., Wu, T., Kodentsov, A., van der Ven, L., de With, G. and van Benthem, R., "Impedance evaluation of permeability and corrosion of al-2024 aluminum alloy coated with a chromate free primer", *Progress in Organic Coatings*, Vol. 65, No. 2, (2009), 257-262.

28. Amiri, M.S. and Kashefi, M., "Investigation of variables affecting impedance plane in eddy current testing of carburized steels", *Journal of materials engineering and performance*, Vol. 20, No. 3, (2011), 476-480.

29. Stupakov, O., "Investigation of applicability of extrapolation method for sample field determination in single-yoke measuring setup", *Journal of Magnetism and Magnetic Materials*, Vol. 307, No. 2, (2006), 279-287.

30. Standard, A., "E975-03: Standard practice for x-ray determination of retained austenite in steel with near random crystallographic orientation", *ASTM, West Conshohocken, PA*, Vol., No., (2008).

31. Davut, K. and Gür, C.H., "Monitoring the microstructural changes during tempering of quenched sae 5140 steel by magnetic barkhausen noise", *Journal of Nondestructive Evaluation*, Vol. 26, No. 2-4, (2007), 107-113.

32. Sheikh Amiri, M. and Kashefi, M., "Application of eddy current nondestructive method for determination of surface carbon content in carburized steels", *NDT & E International*, Vol. 42, No. 7, (2009), 618-621.

Applications of Impedance Plane and Magnetic Differential Permeability in Microstructural Characterization of AISI D2 Tool Steel

S. Kahrobaee, M. Kashefi

Department of Materials Science and Metallurgical Engineering, Engineering Faculty, Ferdowsi University of Mashhad, Mashhad, Iran

چکیده

در پژوهش حاضر از روش‌های الکترومغناطیسی/مغناطیسی حلقه هیسترزیس و جریان گردابی در مشخصه‌یابی فولاد ابزار سردکار D2 که تحت شرایط متفاوت از عملیات کوئنچ و تمپر قرار گرفته، استفاده شده است. به منظور اندازه‌گیری کسر آستنیت باقیمانده در ریزساختار حاصل از عملیات کوئنچ، ۶ نمونه در محدوده دمایی ۱۰۰۰ تا ۱۱۳۰ درجه سـانتی‌گـراد آستنیته شدند. همچنین، نمونه‌هایآستنیته شده‌در دمای ۱۰۸۰ درجه سانتی‌گراد تحت عملیات تمپر در بازه دمـایی ۲۰۰ تـا ۶۵۰ درجه سانتی‌گراد قرار گرفتند تا ریزساختارهای به دسـت آمـده بـا اسـتفاده از روش‌هـای جریـان گردابـی و حلقـه هیسترزیس به صورت غیرمخرب شناسایی شوند. به منظورشناسایی تغییـرات ریزسـاختاری ایجـاد شـده، حرکـت نقطـه امپدانس در صفحه مربوطه و همچنین تغییراتماکزیمم نفوذپذیری تفاضلی به صورت تـابعی از دماهـای آسـتنیته و تمپـر بررسی شد. بررسی‌هابیانگر ارتباط خوبی بین تغییرات ریزساختاری شناسایی شده با روش‌های مخرب (سختی، پراشاشعه ایکس و مشاهدات میکروسکوپی) و خروجی‌های تکنیک‌های غیرمخرب است.

doi: 10.5829/idosi.ije.2015.28.02b.09